それぞれ特徴的な転写因子やサイトカイン，ケモカイン受容体を発現している．通常，これらのThサブセットはバランスを保って存在しているが，そのバランスに破綻が生じると宿主に免疫異常がひき起こされると考えられており，近年，このバランス破綻にTh細胞の分化異常の重要性が注目されている[9]．これに関連して，われわれはHAMにおけるHTLV-1感染細胞が主にTregやTh2細胞に発現するケモカイン受容体CCR4陽性のCD4$^+$T細胞であり，興味深いことにHAMの末梢血CCR4$^+$CD4$^+$T細胞は，炎症性サイトカインIFN-γを産生するTh1細胞様の異常細胞に変化し増加していることを示した[10]．また，HTLV-1由来の機能遺伝子であるtaxやHBZの発現がTregの免疫制御機能の低下を誘導することが報告されている[11][12]．このようにHAM患者におけるCCR4$^+$CD4$^+$T細胞は，HTLV-1感染によって機能的な異常を伴って増加しており，Thバランスにも影響を与え，HAM病態形成に重要な役割を果たしていることが示唆されている．

HAMにおける炎症の慢性化機構

HAM脊髄病巣の病理所見では，小血管周囲の炎症細胞の浸潤やIFN-γなどの炎症性サイトカインの発現を認め，持続的な炎症が起こっていることが示されてきた[13]．さらに，HTLV-1感染細胞についてin situ PCR法を用いて解析されており，HTLV-1の感染は浸潤したT細胞にのみ確認され，周辺の神経細胞やグリア細胞には確認されていない[14]．以上から，HAMの脊髄病巣ではHTLV-1感染T細胞に起因する慢性炎症が存在すると考えられているが，その炎症の形成および慢性化機構については不明であった．

最近，われわれはHAM患者脊髄における炎症の慢性化が脊髄局所での病的なケモカイン産生を軸とする炎症のポジティブフィードバックループに起因するという仮説を立て，HAMの病態の主軸となるケモカインの同定を試みた[15]．その結果，HAM患者髄液中で高値を示した炎症性ケモカインの中で，Th1細胞に発現するCXCR3のリガンドであるCXCL10のみが，血清中よりも髄液中で高い濃度勾配を示し，髄液CXCL10濃度は髄液細胞数と相関していた．また，HAM患者の髄液や脊髄病変には，CXCR3を発現する細胞（主にCD4$^+$T細胞とCD8$^+$T細胞）が多数を占めており，CXCL10によりCXCR3陽性細胞が優先的に脊髄に遊走していることが示された．さらに，CXCL10により遊走するCXCR3$^+$CD4$^+$T細胞は，その一部にHTLV-1感染を認め，HTLV-1感染細胞の脊髄への遊走にもCXCL10が重要な役割を果たしていることが示唆された．また，患者脊髄病変部におけるCXCL10の主な産生細胞はアストロサイトであることが判明し，アストロサイトは患者由来CD4$^+$T細胞からのIFN-γ産生によりCXCL10を過剰産生することが示された．以上より，HAMの脊髄病変では浸潤したHTLV-1感染細胞から産生されるIFN-γによってアストロサイトからのCXCL10産生を刺激し，そのCXCL10はCXCR3陽性の感染CD4$^+$T細胞やCD8$^+$T細胞などの炎症細胞の脊髄への遊走を促し，それらの細胞がIFN-γを産生してアストロサイトからのさらなるCXCL10産生を刺激するという，炎症のポジティブフィードバックループ（IFN-γ-CXCL10-CXCR3ループ）の形成が炎症の慢性化機構の主軸であり，HAMの脊髄病巣の形成・維持に重要な役割を果たしていると考えられる（図2）[15]．

HAMに対する抗CCR4抗体療法の開発

上述したようなこれまでのHAMの病態研究や臨床的なデータから，HAM患者においてHTLV-1感染細胞の劇的な低下とその維持を実現することは，病態ならびに長期予後の改善につながることが予想され，HAMにおいて感染細胞を標的とした薬剤開発の必要性が高い．そのためこれまでも世界中の研究者がHAMに対する抗ウイルス療法の開発を試みてきた．逆転写酵素阻害薬やプロテアーゼ阻害薬などは*in vitro*での感染阻害作用が示され，実際にHAM患者を対象として臨床試験が実施されたが，ウイルス量の減少効果はまったく得られず，治療効果に乏しかった[16][17]．HTLV-1は，エイズウイルスや肝炎ウイルスなどとは異なり転写レベルが低いため血清中にウイルスが存在せず，また感染細胞はオリゴクローナルな集団を形成する特徴を有しているので[18][19]，ウイルス量の制御には異なった戦略，たとえば感染細胞を特異的に攻撃・死滅させる

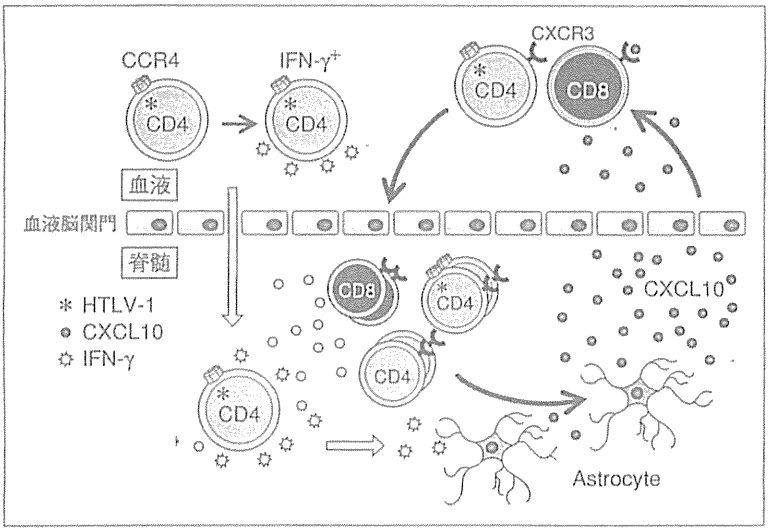

図2　HAM感染細胞を起因とした炎症のポジティブフィードバックループ

抗体療法などの開発が必要と考えられる．

そこでわれわれは，HAM患者においてHTLV-1が主にCCR4陽性T細胞に感染し，その細胞機能が炎症促進的になっていると報告したことなどを踏まえ[10]，CCR4抗原を標的として抗体依存性細胞障害活性を示すヒト化抗CCR4抗体製剤mogamulizumab(KW-0761)に着目して研究を進めた．KW-0761はわが国で開発され，HTLV-1感染者より発症する成人T細胞白血病・リンパ腫(ATLL)の治療薬として最近承認された薬剤である．われわれはKW-0761を用いて，HAM患者の血液・髄液由来細胞における感染細胞殺傷効果，自発的細胞増殖抑制効果，炎症性サイトカイン産生抑制効果等を証明し，CCR4がHAMの有用な治療標的分子であることを示した[20]．さらに，これまでのKW-0761を用いた他の治験において，健康成人やATL等患者に対する安全性が確認されており，またATL患者におけるCCR4陽性ATL細胞の劇的な減少効果が示されていることから[21][22]，KW-0761は，HAMに対する安全かつ有効な治療薬になりうると考えられた．そこで，KW-0761のHAMに対する医師主導治験の実施を計画した．試験デザインは，HAMが希少難病であることを踏まえ，できるだけ早期に新薬承認がなされるよう，第I/IIa相試験と工夫した．治験プロトコールの内容は，対象を既存治療で効果不十分なHAM患者とし，主要評価項目は安全性で，用量制限毒性の発現状況に基づき，最大耐用量を明らかにし，同時に薬物動態について検討する．また副次的に，抗感染細胞効果や歩行時間の非増悪期間などを検討して有効性を探索する．すでに治験プロトコールに関して医薬品医療機器総合機構(PMDA)の対面助言を終了しており，厚生労働省科学研究費補助金の助成のもと，2013年12月から治験を開始した．今回実施するKW-0761の治験が成功すれば，これまで有効な治療法が確立していない神経難病であるHAMの長期予後改善に結びつく，日本発の革新的な治療薬の創出につながり，HAMの治療にパラダイムシフトをもたらすことが期待される．

おわりに

HAMは長期にわたり障害を強いられる疾患で，患者の苦痛は大変深刻であり，一刻も早い有効な治療法の開発が切望されている．HAMのこれまでの研究により，感染細胞を標的とした薬剤開発はHAMの根本的な治療薬となることが期待されてきたが，これまで実現されなかった．ところが，近年の分子レベルでの病態解明やわが国の研究者によるバイオテクノロジー技術の進展などにより，その実現の可能性を探る臨床試験実施の機会が得られる段階にまで発展してきている．HAMは慢性炎症性疾患であるので，薬剤開発においては，安全性や長期忍容性などを

十分に配慮することが求められる．現状では，抗CCR4抗体製剤がHTLV-1感染細胞の劇的な減少を期待できる唯一の薬剤であるので，安全に治療可能な用量や用法などの決定に向け，慎重かつ綿密な臨床試験の実施を重ね，有用なエビデンスを蓄積していくことが重要と考える．

近年ではHAMの治療標的と成りうる細胞や分子の理解が進んできており，今後，新薬につながる成果がさらに得られることが期待される．また，ウイルス感染症と脊髄の慢性炎症の制御が，当面のHAM治療の達成すべき課題であるが，最近注目を集めている再生医療の応用も必要と考えられる．HAM患者は世界中に存在するが，先進国の中で患者数が多いのは日本のみであり，HAMの新薬開発研究におけるわが国の役割は大きい．

文　献

1) Osame M, Usuku K, Izumo S, et al. HTLV-I associated myelopathy, a new clinical entity. Lancet 1986 ; 1 : 1031.
2) Yamano Y, Sato T, Ando H, et al. [The current and future approaches to the treatment of HTLV-1-associated myelopathy/tropical spastic paraparesis (HAM/TSP)]. Nihon Rinsho 2012 ; 70 : 705. Japanese.
3) Nakagawa M, Izumo S, Ijichi S, et al. HTLV-I-associated myelopathy : analysis of 213 patients based on clinical features and laboratory findings. J Neurovirol 1995 ; 1 : 50.
4) Martin F, Fedina A, Youshya S, et al. A 15-year prospective longitudinal study of disease progression in patients with HTLV-1 associated myelopathy in the UK. J Neurol Neurosurg Psychiatry 2010 ; 81 : 1336.
5) Buyse M, Sargent DJ, Grothey A, et al. Biomarkers and surrogate end points–the challenge of statistical validation. Nat Rev Clin Oncol 2010 ; 7 : 309.
6) Olindo S, Lezin A, Cabre P, et al. HTLV-1 proviral load in peripheral blood mononuclear cells quantified in 100 HAM/TSP patients : a marker of disease progression. J Neurol Sci 2005 ; 237 : 53.
7) Takenouchi N, Yamano Y, Usuku K, et al. Usefulness of proviral load measurement for monitoring of disease activity in individual patients with human T-lymphotropic virus type I-associated myelopathy/tropical spastic paraparesis. J Neurovirol 2003 ; 9 : 29.
8) Sato T, Coler-Reilly A, Utsunomiya A, et al. CSF CXCL10, CXCL9, and Neopterin as Candidate Prognostic Biomarkers for HTLV-1-Associated Myelopathy/Tropical Spastic Paraparesis. PLOS Neglected Tropical Diseases 2013 ; 7 : e2479.
9) Zhou X, Bailey-Bucktrout SL, Jeker LT, et al. Instability of the transcription factor Foxp3 leads to the generation of pathogenic memory T cells in vivo. Nat Immunol 2009 ; 10 : 1000.
10) Yamano Y, Araya N, Sato T, et al. Abnormally high levels of virus-infected IFN-gamma$^+$ CCR4$^+$ CD4$^+$ CD25$^+$ T cells in a retrovirus-associated neuroinflammatory disorder. PLoS One 2009 ; 4 : e6517.
11) Yamano Y, Takenouchi N, Li HC, et al. Virus-induced dysfunction of CD4$^+$CD25$^+$ T cells in patients with HTLV-I-associated neuroimmunological disease. J Clin Invest 2005 ; 115 : 1361.
12) Yamamoto-Taguchi N, Satou Y, Miyazato P, et al. HTLV-1 bZIP Factor Induces Inflammation through Labile Foxp3 Expression. PLoS Pathog 2013 ; 9 : e1003630.
13) Izumo S, Umehara F, Osame M. HTLV-I-associated myelopathy. Neuropathology 2000 ; 20 : S65.
14) Matsuoka E, Takenouchi N, Hashimoto K, et al. Perivascular T cells are infected with HTLV-I in the spinal cord lesions with HTLV-I-associated myelopathy/tropical spastic paraparesis : double staining of immunohistochemistry and polymerase chain reaction in situ hybridization. Acta Neuropathol 1998 ; 96 : 340.
15) Ando H, Sato T, Tomaru U, et al. Positive feedback loop via astrocytes causes chronic inflammation in virus-associated myelopathy. Brain 2013 ; 136 : 2876.
16) Taylor GP, Goon P, Furukawa Y, et al. Zidovudine plus lamivudine in Human T-Lymphotropic Virus type-I-associated myelopathy : a randomised trial. Retrovirology 2006 ; 3 : 63.
17) Macchi B, Balestrieri E, Ascolani A, et al. Suscepti-

bility of primary HTLV-1 isolates from patients with HTLV-1-associated myelopathy to reverse transcriptase inhibitors. Viruses 2011 ; 3 : 469.

18) Wattel E, Vartanian JP, Pannetier C, et al. Clonal expansion of human T-cell leukemia virus type I-infected cells in asymptomatic and symptomatic carriers without malignancy. J Virol 1995 ; 69 : 2863.

19) Cavrois M, Leclercq I, Gout O, et al. Persistent oligoclonal expansion of human T-cell leukemia virus type 1-infected circulating cells in patients with Tropical spastic paraparesis/HTLV-1 associated myelopathy. Oncogene 1998 ; 17 : 77.

20) 国際出願番号：PCT/JP2013/068296，発明者：山野嘉久．A THERAPEUTIC METHOD AND MEDICAMENT FOR HTLV-1 ASSOCIATED MYELOPATHY (HAM)．国際出願日：2013年7月3日．

21) Yamamoto K, Utsunomiya A, Tobinai K, et al. Phase I study of KW-0761, a defucosylated humanized anti-CCR4 antibody, in relapsed patients with adult T-cell leukemia-lymphoma and peripheral T-cell lymphoma. J Clin Oncol 2010 ; 28 : 1591.

22) Ishida T, Joh T, Uike N, et al. Defucosylated anti-CCR4 monoclonal antibody (KW-0761) for relapsed adult T-cell leukemia-lymphoma : a multicenter phase II study. J Clin Oncol 2012 ; 30 : 837.

* * *

平成24年度厚生労働科学研究費補助金（医療技術実用化総合研究事業）

第3回早期臨床試験国際会議

— 患者を対象とした早期臨床試験 —

希少な慢性進行性の神経難病HAMにおける治療有効性評価モデルの探索

山野　嘉久

臨床評価　別刷

Vol.41, No.3　2014

臨床評価　41巻3号　2014

希少な慢性進行性の神経難病HAMにおける治療有効性評価モデルの探索

Search for a model of drug efficacy for a rare chronic progressive neurological disease HAM

山野　嘉久
Yoshihisa Yamano
聖マリアンナ医科大学難病治療研究センター病因・病態解析部門
Department of Rare Diseases Research, Institute of Medical Science, St. Marianna University School of Medicine

1. HAMとは

我々は希少難病，特に希少神経難病をターゲットに研究を進めています．臨床試験に取り組んでおられる先生方とより交流を深め，一緒に治療薬を開発していけることを望んでいます．本日はHAM（HTLV-1 Associated Myelopathy：HTLV-1関連脊髄症）という希少神経難病についての治療効果評価指標の確立に向けた研究の内容を紹介させていただきます．HAMは，rareでchronicという難しい疾患です．

まず，HAMとはHTLV-1感染者の一部に発症する神経難病です（Fig. 1）．HTLV-1とは，ヒトのT細胞に白血病を起こすウイルス1型（Human T-cell Leukemia Virus type-1）のことで，世界共通でHTLV-1と呼ばれています．日本には100万人以上の感染者がおり，すなわち約100人に1人

Fig. 1　HTLV-1関連脊髄症（HAM）とは

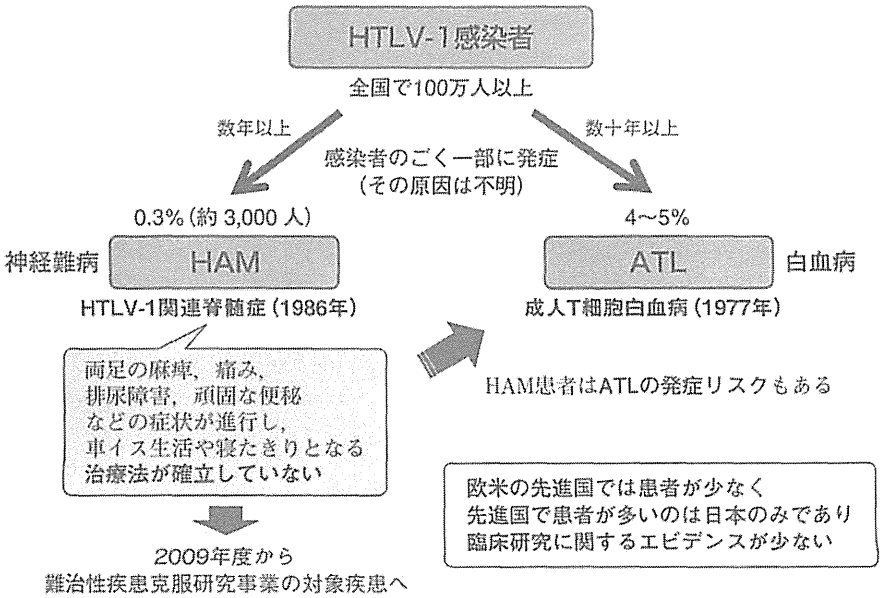

が感染しています．HTLV-1の感染者は，その約0.3％にHAMを発症します．日本には約3,000人のHAM患者がいるといわれています．

このウイルスは感染者の4～5％に致死的な成人T細胞白血病（Adult T-cell Leukemia：ATL）を引き起こし，残念ながらATLの治療法は確立されていません．一方，HAMは脊髄が傷害されるので両足の麻痺，痛み，排尿障害，頑固な便秘などの症状が進行し，重症な方は車イス生活や寝たきりになる病気です．残念ながらHAMも治療法が確立されておらず，2009年に国の難病に指定されています．

HTLV-1感染症やHAMは欧米の先進国で感染者，患者が少ないという特徴があります．先進国で患者が多いのは日本のみで，欧米での臨床研究に関するエビデンスがとても少ないことが，他の難病と比較してこの病気の研究が進展しにくい大きな原因の1つとなっています．したがって，日本で積極的に取り組むことが強く求められています．

2. HAMのバイオマーカー

HAMの治療は，その臨床経過や疾患活動性を踏まえて治療戦略を考える必要があると思われます（Fig. 2）．HAM患者の経過は様々という特徴があるので，できるだけ早く疾患活動性を判定し，経過や疾患活動性に応じた治療を実施することが望まれます．重要なことは，治療の最終目標が長期予後の改善であることを認識することで，これを見据えた治療戦略が必要です．そのためには，長期予後や経過と相関するバイオマーカーの情報が必要です．そして，経過や疾患活動性に応じた治療成績に関するエビデンスを作ることがさらに必要と思います．

今日のセッションのテーマはサロゲートエンドポイントですので，HAMのサロゲートエンドポイントについて考えてみたいと思います（Fig. 3）．希少難病であるHAMでは，まだサロゲートエンドポイントが確立されていませんが，これからど

Fig. 2　HAMの経過の特徴を踏まえた治療の考え方（案）

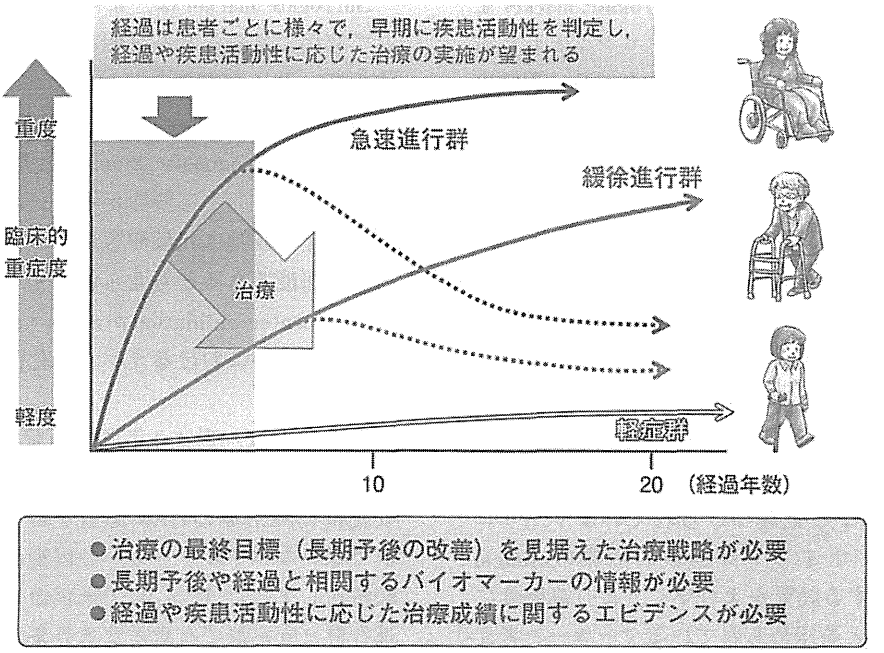

Fig. 3　HAMにおける治療効果判定方法に関する課題

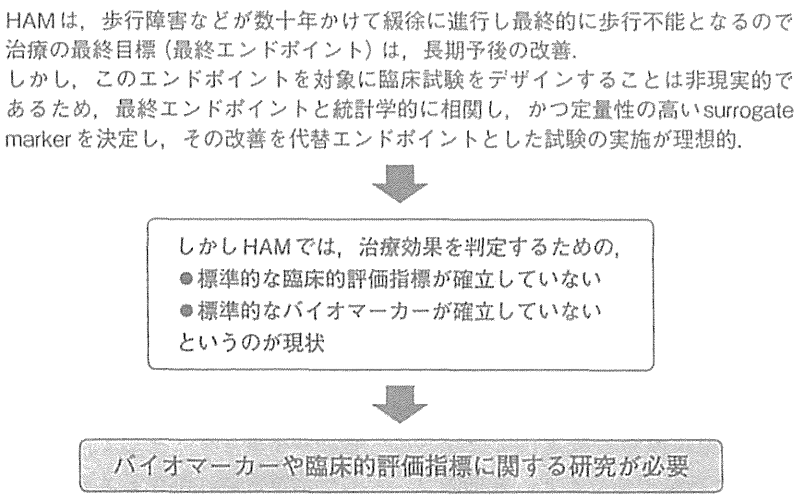

のようにして確立していくのか，今日は特にバイオマーカーに焦点をあててお話しします．HAMは，歩行障害などが数十年かけて緩徐に進行し，最終的に歩行不能となりますので，治療の最終目標，true endpointは長期予後の改善です．しかし，これを標的に臨床試験をデザインすることは非現実的です．したがって，true endpointと統計学的に相関し，かつ定量性の高いsurrogate markerを決定し，その改善を代替エンドポイントとした試験の実施が求められます．しかしながら，現時点では治療効果を判定するための標準的な臨床的評価指標すら確立しておらず，標準的なバイオマーカーも確立していないのが現状であり，バイオマーカーや臨床的評価指標に関する研究をしっかりと進めていかなければならないのです．

今日は，そのための取り組みを紹介します．バイオマーカーには，prognostic biomarkerとpredictive biomarker，そしてサロゲートエンドポイントがあります．Prognostic biomarkerは予後を予測する因子，predictive biomarkerは治療効果を予測する因子と定義づけられています．サロゲートエンドポイントは実験的治療のclinical endpointに対する効果をより早く，より高感度に評価できることを求められているマーカーと考えられています．

サロゲートエンドポイントはtrue endpointが予測可能でないといけません．Surrogate markerに対する治療効果がtrue endpointに対する効果と相関していることを示さないといけません．同定と並行し，臨床試験を通し，きちんと証明する作業が必要になります．

Surrogate markerは，まずprognostic markerとして有用であることを証明することが求められますので，我々は最近，HAMについて，candidate prognostic biomarkerをみつける取り組みを進めています．Prognostic biomarkerは将来サロゲートエンドポイントにつながるマーカーと思われますが，その候補は比較的容易に，後ろ向き研究でも同定可能であると考えられます．しかしその後にmulticenter validationかcross-validationが必要で，臨床試験におけるランダム化前向き試験が必要です．

最近我々は，過去4年間で重症度が3 grade以上悪化する進行群と1 grade以下しか悪化しない安定群に無治療のHAM患者を群分けし，この2群で様々なバイオマーカーの候補となる分子を比較解析しました（Fig. 4）．末梢血のウイルス量は進行群と安定群で有意差がありましたが，もっと

Fig. 4　HAMのprognostic biomarker候補の同定

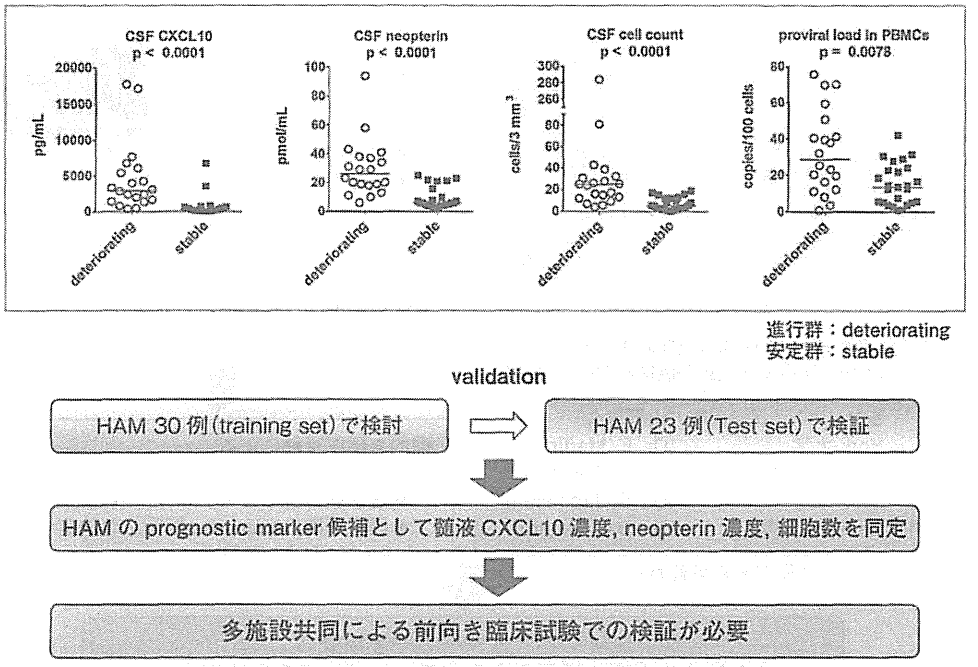

Sato T, Coler-Reilly A, Utsunomiya A, Araya N, Yagishita N, Ando H, Yamauchi J, Inoue E, Ueno T, Hasegawa Y, Nishioka K, Nakajima T, Jacobson S, Izumo S, Yamano Y. CSF CXCL10, CXCL9, and neopterin as candidate prognostic biomarkers for HTLV-1-Associated Myelopathy/Tropical Spastic Paraparesis. *PLoS Negl Trop Dis.* 2013 ; 7(10) : e2479.

高い有意差があったのは，髄液中のCXCL10 (C-X-C motif chemokine 10) というchemokine濃度とneopterin濃度，そして細胞数でした．ただし，細胞数は感度が低いことが判明しています (data not shown)．この髄液CXCL10濃度とneopterin濃度がよいprognostic markerであることを，無治療30例のtraining setで証明し，さらに，引き続いて来院した異なる23例の無治療HAM患者で検証して，全く同じ結果が出ていますので，かなり信頼性の高い結果であることが示されました．

3. HAMの国際共同臨床研究チーム

このようにretrospective studyで，candidate prognostic markerを同定しましたが，次に，多施設による前向き臨床試験での検証が必要になってきます．そこで我々は，国際共同臨床研究チームを結成しています (Fig. 5)．アメリカのNIH (National Institutes of Health)，イギリス，ブラジル，日本の研究者が参加し，clinical trialを推進するHAM clinical trial study group (HAM-CTSG) を結成しています．国際共同で実施することによって高いエビデンスレベルが得られます．しかも前向きの臨床試験によってバイオマーカーや治療効果を検討し，国際的なコンセンサスを得ていこうと考えています．そしてこの結果は，臨床現場に還元できる重要なエビデンスを創出できるのではないかと考えています．サロゲートエンドポイントはtrue endpointが予測可能でないといけません．すなわち，surrogate markerに対する治療効果がtrue endpointに対する効果と相関していることを示さないといけませんので，多施設の前向き臨床試験をこのようなコンソーシアムで複数実施していくことによって，HAMのサロゲートエンドポイントの確立に向けて研究を進めていきたいと考えています．

Fig. 5　HAMの国際共同臨床研究チームを結成

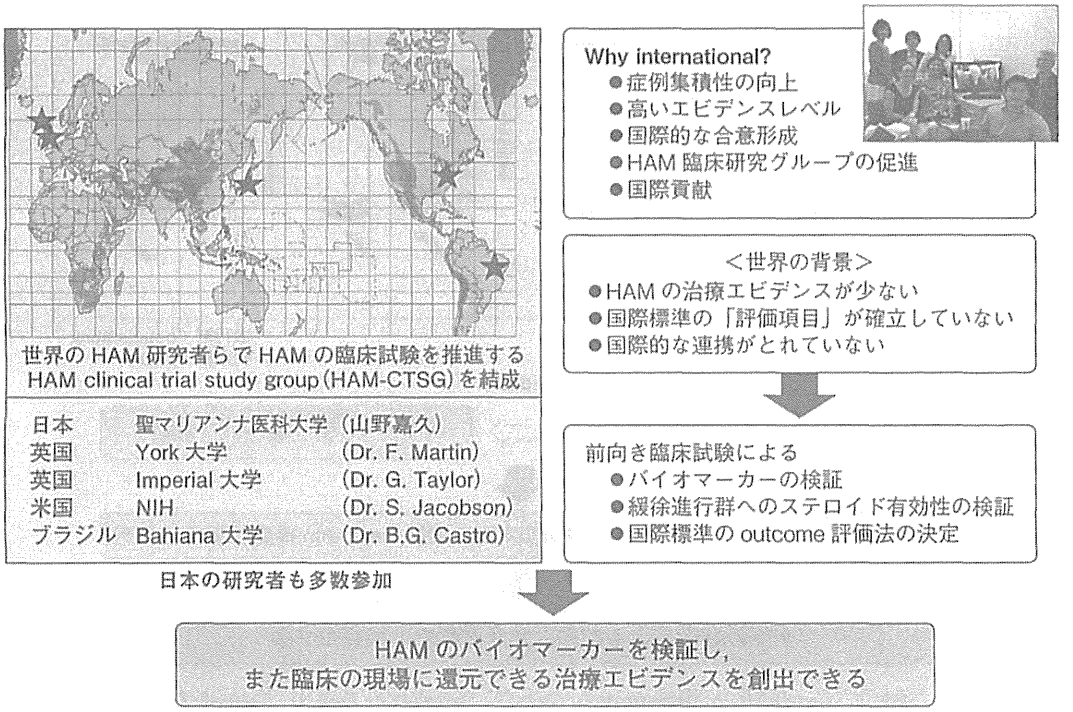

＊　　＊　　＊

Hindawi Publishing Corporation
BioMed Research International
Volume 2014, Article ID 648021, 6 pages
http://dx.doi.org/10.1155/2014/648021

Clinical Study

Perfusion in the Tissue Surrounding Pancreatic Cancer and the Patient's Prognosis

Yoshihiro Nishikawa,[1] Yoshihisa Tsuji,[1] Hiroyoshi Isoda,[2] Yuzo Kodama,[1] and Tsutomu Chiba[1]

[1] *Department of Gastroenterology and Hepatology, Kyoto University Graduate School of Medicine, 54 Kawara-cho, Shogoin, Sakyo-ku, Kyoto 606-8507, Japan*
[2] *Department of Radiology, Kyoto University Graduate School of Medicine, 54 Kawara-cho, Shogoin, Sakyo-ku, Kyoto 606-8507, Japan*

Correspondence should be addressed to Yoshihisa Tsuji; ytsuji@kuhp.kyoto-u.ac.jp

Received 9 April 2014; Revised 15 July 2014; Accepted 31 August 2014; Published 11 September 2014

Academic Editor: Luca Volterrani

Objective. The objective was to investigate the relationship between prognosis in case of pancreatic cancer and perfusion in tissue surrounding pancreatic cancer using perfusion CT. *Methods.* We enrolled 17 patients diagnosed with inoperable pancreatic adenocarcinoma. All patients were examined by perfusion CT and then underwent chemotherapy using gemcitabine. The time density curve (TDC) of each CT pixel was analyzed to calculate area under the curve (AUC) and blood flow (BF) using a mathematical algorithm based on the single-compartment model. To measure the AUC and BF of tumor (AUC_T and BF_T) and peritumoral tissue (AUC_{PTT} and BF_{PTT}), regions of interest were manually placed on the cancer and in pancreatic tissue within 10 mm of proximal pancreatic parenchyma. Survival days from the date of perfusion CT were recorded. Correlation between AUC or BF and survival days was assessed. *Results.* We found a significant correlation between AUC_{PTT} or BF_{PTT} and survival days ($P = 0.04$ or 0.0005). Higher AUC_{PTT} or BF_{PTT} values were associated with shorter survival. We found no significant correlation between AUC_T or BF_T and survival. *Conclusions.* Our results suggest that assessments of perfusion in pancreatic tissue within 10 mm of proximal pancreatic parenchyma may be useful in predicting prognosis.

1. Introduction

Pancreatic ductal adenocarcinoma (PDA) is the fourth leading cause of cancer-related death in the United States [1]. PDA is nearly universally lethal, with 5-year survival rates of less than 5% [1–3]. This poor prognosis is related to early diagnostic difficulties; the disease in more than 80% of patients at the diagnostic stage is already metastatic or locally advanced [2]. Inoperable patients typically undergo gemcitabine-based chemotherapies but with limited effectiveness [4].

Desmoplastic stroma is a histopathological characteristic of PDA [5]. The lack of adequate vasculature due to the presence of desmoplastic stroma is believed to be among the factors leading to resistance to conventional chemotherapies. The low density of vasculature causes poor perfusion, limiting the transport of the anticancer drug from vessel to tissue [6]. Tumor-associated stroma has been reported to increase chemoresistance in PDA [7]. Stromal accumulation of hyaluronan in a mouse model of PDA impaired both vascular function and drug delivery [8]. Accumulating evidence suggests the importance of tumor-associated stroma and vasculature in PDA.

As reported in previous studies, patients with pancreatic cancer may have a history of chronic pancreatitis [9]. Additionally, patients with PDA often have cancer-related pancreatitis [5]. The microstructure of the pancreas in PDA patients tends to be highly desmoplastic, resulting in reduced tissue perfusion. However, recent reports based on mouse PDA model indicate increased perfusion in the tissue surrounding PDA [10]. In human, Radu et al. report that cancer surrounding vasculature was changed due to development of cancer [11]. These studies suggest that perfusion in the tissue surrounding cancer sites may be related to cancer activity. This possibility suggests a need to investigate the relationship

between prognosis and perfusion in the tissue surrounding cancer. However, tissue vasculature can be ascertained only through intensive examination (e.g., of pathological specimens), a process that presents major difficulties. For these reasons, how or whether perfusion in the tissue surrounding a cancer relates to cancer activity remains poorly understood.

Recent reports indicate perfusion CT can be used to evaluate tissue vasculature, thereby allowing noninvasive perfusion measurements. Perfusion CT is a type of dynamic CT capable of measuring tissue perfusion based on analyses of time-density curve (TDC) derived from a bolus injection of contrast material. Perfusion CT is reported to be able to obtain nonmorphological information and is valuable for diagnosis in some organs [12]. In the study described here, we applied perfusion CT to investigate the relationship between patient prognosis and perfusion in the tissue surrounding a pancreatic cancer using perfusion CT.

2. Materials and Methods

2.1. Patients. Between December 2008 and February 2011, our pilot study enrolled 17 patients with inoperable pancreatic adenocarcinoma (PDA). We obtained written informed consent from all patients, and the research protocol was approved by the corresponding institutional review boards. Patients with histologically diagnosed pancreatic adenocarcinoma judged to be inoperable metastatic or locally advanced cancer were enrolled in this study. Diagnoses of locally advanced cancer and/or metastasis were made by a single board-certificated radiologist based on CT and/or MRI findings. All patients were treated using gemcitabine. Patients demonstrating intolerance for the contrast material for dynamic CT were excluded from the study. Our medical chart recorded age, gender, survival days from the date on which perfusion CT was performed, TNM [13], and stage of cancer [14].

2.2. Perfusion CT Protocol and Analysis. All patients were examined by perfusion CT and then underwent chemotherapy using gemcitabine. We used multidetector CT (Aquilion 64, Toshiba Medical Systems, Tochigi, Japan) to perform pancreatic perfusion CT [15]. The scanning tube voltage and current were 80 kVp and 40 mA, respectively, resulting in radiation exposures of 60–100 mGy (CTDIvol) [16]. For initial localization of the tumor, a CT study of the abdomen was obtained without contrast material enhancement during a breath hold at the end of expiration; then the CT perfusion examination of the selected area was performed in a single breath hold at end expiration. A supervising radiologist identified the tumor and then placed the predefined scan volume in the z-axis to cover the lesion for the CT perfusion study. We referred to other image data sets (e.g., US and MRI) for patients for whom such data sets existed to help identify cancer sites. To reduce respiratory artifacts, a belt over the abdomen was used and patients were instructed to breathe gently during the scan acquisition.

Stationary CT scans of four slices were acquired every 0.5 seconds over a period of 54 seconds following intravenous bolus injections of 40 mL of contrast material (Iomeprol 350 mg/mL (molecular weight, 777 kDa)) at 4 mL/second. Perfusion CT scan began 3 seconds after the start of injection. We injected iodinate contrast material through a 20-gauge intravenous cannula, followed by injection of 50 mL of saline solution, in a right cubital vein. The TDC of each CT pixel was analyzed to calculate the area under the curve (AUC) and blood flow (BF) using a mathematical algorithm based on a single-compartment model [17, 18] on workstation (ziostation2, Ziosoft, Tokyo, Japan) (Figures 1(a)–1(c)) [19].

After all of the images were loaded on a dedicated work station, the tumor was defined. TDC of the arterial input was measured by placing a circular region of interest (ROI) within the aorta on a selected image. The arterial TDC was derived automatically by the software. The AUC and BF of tumor (AUC_T and BF_T) and peritumoral tissue (AUC_{PTT} and BF_{PTT}) were obtained within a freehand ROI drawn both over the tumor itself and over pancreatic tissue within 10 mm of the juxtaposed proximal pancreatic parenchyma. We drew the largest possible single ROI that could be drawn around each tumor and peripancreatic tissue while still excluding necrosis, calcifications, and cystic or any hemorrhagic areas. The perfusion values were obtained from the parametric maps generated with the software package. Image analysis was performed in consensus by single radiologist (with 11-year experience in abdominal perfusion CT).

2.3. Statistical Analysis. We recorded survival days from the date of perfusion CT by chart review and assessed the correlation between AUC or BF and survival days by Spearman's rank correlation test. Data is presented as median (range); P values of less than 0.05 were deemed significant. The software used for statistical analysis was JMP (version 9.01, SAS Institute, NC).

3. Results

3.1. Patients. Between December 2008 and February 2011, our pilot study enrolled 17 patients with inoperable pancreatic adenocarcinoma (PDA). Of these patients, 12 (70.6%) were male and 5 (29.4%) were female. The median age was 63 (36–78). Median survival days from the date on which perfusion CT was performed were 298 days (57–914) (Table 1). According to TNM classification, patients with T4 (tumor involves celiac axis or superior mesenteric artery) and T3 (tumor extends beyond pancreas but no celiac or superior mesenteric artery involvement) [13] numbered 14 (82.4%) and 3 (17.6%), respectively. According to the Japanese classification, 8 patients were stage IVa (locally advanced cancer) and 9 patients were stage IVb (metastatic cancer) [14]. All patients were treated with gemcitabine.

3.2. Perfusion Data and Survival Days. We investigated area size, BF, and AUC of TDC in tumors and peritumoral tissue (Table 2). Area size was measured using the ROI on a workstation. We also used this ROI to measure BF and AUC. The area size of pancreatic tumor area and peritumoral area (average ± SD), respectively, were 17.7 ± 24.1 (cm^2) and 1.9 ± 1.1 (cm^2). BF_{PTT}, AUC_{PTT}, BF_T, and AUC_T, respectively, were

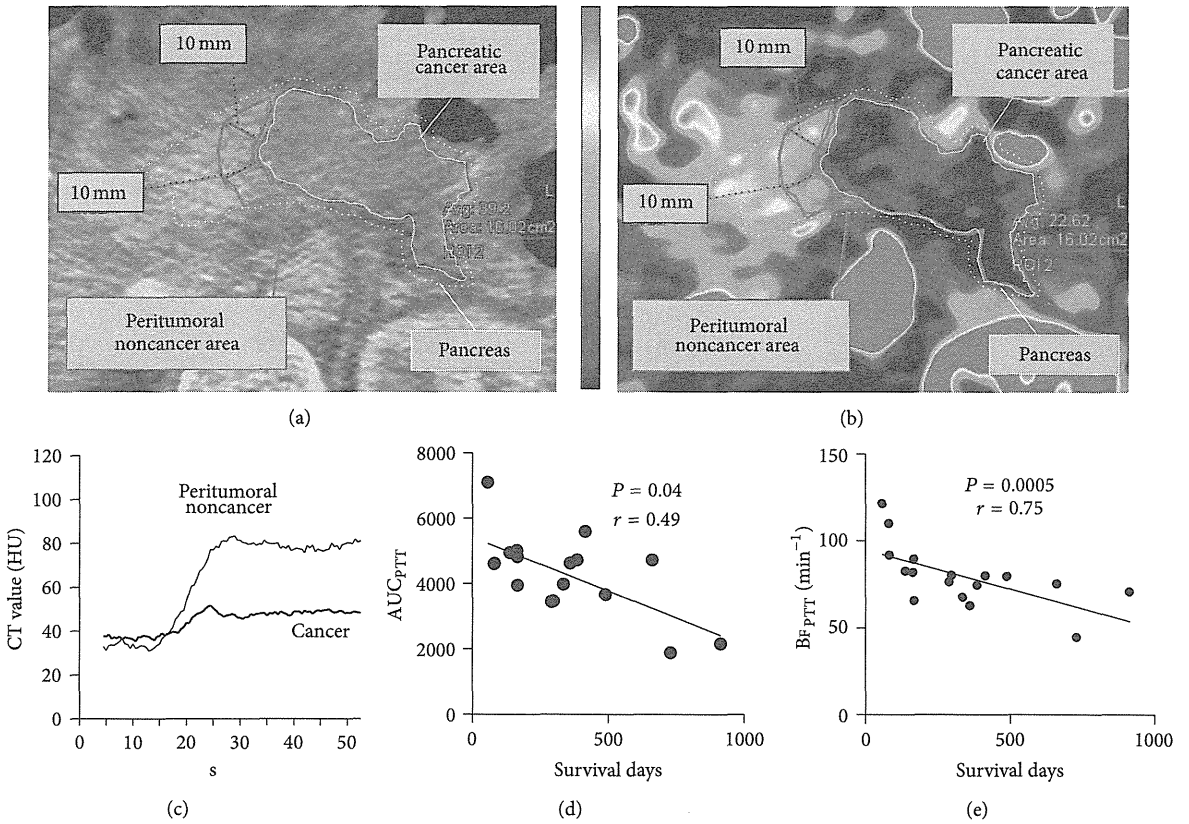

FIGURE 1: Analysis of pancreatic perfusion image. We analyzed the CT image dataset (of which Panel (a) is an excerpt) to obtain Panel (b). Panels (a) and (b) are magnified by the same factor. Panel (b) is a perfusion image of pancreatic blood flow (BF). Pancreatic BF is indicated by the scale on the left. Colors shift from black to red with increasing BF. The pancreatic regions of interest (ROIs) in Panels (a) and (b) have the same size and location. Panel (c) shows time-density curves for peritumoral noncancer (PTT) and cancer (T) sites for Panels (a) and (b). Panels (d) and (e) show the relationship between pancreatic AUC_{PTT} or BF_{PTT} and survival days, respectively.

TABLE 1: Background information for patients enrolled.

Number	Sex (M/F)	Age (age)	Survival days from date PCT performed	TNM	Stage
1	M	78	57	T4N2M1	IVb
2	M	61	298	T4N0M0	IVa
3	M	59	360	T4N3M1	IVb
4	F	78	80	T3N1M1	IVb
5	M	36	167	T3N0M1	IVb
6	F	63	138	T4N2M0	IVb
7	F	65	662	T4N1M0	IVa
8	M	61	82	T4N0M1	IVb
9	M	49	290	T4N0M0	IVa
10	M	55	166	T4N0M1	IVb
11	F	67	386	T4N0M0	IVa
12	M	64	914	T4N1M0	IVa
13	M	66	415	T4N0M0	IVa
14	M	65	730	T4N0M1	IVb
15	M	46	164	T4N0M0	IVa
16	F	66	490	T3N0M1	IVb
17	M	46	336	T4N0M0	IVa
	12/5	63.0 ± 11.1	298 ± 246		

Figures (median ± SD) for age and survival days from date perfusion CT (PCT) performed appear at the bottom of each column.

Table 2: Area, blood flow, and area under curve with injection of contrast material in pancreatic tumor and peritumoral tissue.

Number	Area of pancreatic tumor (cm^2)	Area of peritumoral tissue (cm^2)	BF_{PTT} (min^{-1})	AUC_{PTT}	BF_T (min^{-1})	AUC_T
1	28.8	25.2	121.4	3511	999	1618
2	98.6	36.9	80.15	2946	4004	3337
3	7.4	12.63	62.65	2173	1376	2529
4	3.8	44.9	109.9	3706	2321	2689
5	4.0	19.15	65.6	1786	1879	2604
6	27.8	24.16	82.48	2593	2108	2256
7	3.0	36.22	75.2	3277	1682	2344
8	22.2	20.9	91.7	3791	645	3791
9	2.9	27.4	76.4	2800	1750	2988
10	19.1	18.6	89.52	3340	966	1204
11	1.6	34.47	74.35	3527	3012	2622
12	7.5	11.6	70.8	2778	386	1796
13	2.7	39.1	79.9	2763	1638	2779
14	3.7	26.3	44.4	1413	844	1258
15	16.0	23.9	81.78	3312	1959	1909
16	44.4	49.6	79.5	1931	3430	1741
17	7.3	26.9	67.5	3717	289	2537
	17.7 ± 24.1	1.9 ± 1.1	79.6 ± 17.5	2904 ± 726	28.1 ± 10.7	2353 ± 701

BF_{PTT} and BF_T, respectively, represent blood flow (BF) of peritumoral tissue (PTT) and pancreatic tumor (T) as determined by perfusion CT. AUC_{PTT} and AUC_T, respectively, represent area under curve (AUC) with bolus injection of contrast media for PTT and T. Measurement results (average ± SD) appear at bottom of each column.

79.6 ± 17.5 (min^{-1}), 2904 ± 726, 28.1 ± 10.7 (min^{-1}), and 2353 ± 701. We observed significant correlation between AUC_{PTT} or BF_{PTT} and survival days from the date on which perfusion CT was performed ($P = 0.04$ or 0.0005). Higher AUC_{PTT} or BF_{PTT} values were associated with shorter survival (Figures 1(d) and 1(e)). We found no significant correlation between BF_T or AUC_T and survival (Figures 2(a) and 2(b)).

4. Discussion

In this study, we investigated the relationship between patient prognosis and perfusion in pancreatic cancer and tissue surrounding cancer using perfusion CT. In startling finding, survival days correlated significantly with peritumoral blood flow but not with tumor blood flow.

The results suggest that prognosis is related to increased perfusion in tissue surrounding cancer. Using MR perfusion technique in animal model, Olive et al. have shown that blood flow of peripheral tissue of pancreatic cancer increased [10]. Radu et al. have reported that follicle-stimulating hormone receptor (FSHR) was selectively expressed on the surface of peritumoral vessels [11]; in their report, the authors speculate that FSHR expression may induce VEGF and VEGF receptor 2 signaling in tumor endothelial cells and thereby promote increased vascularization. Pancreatic cancer may alter peritumoral microstructures before invading normal tissue. Thus, increased peritumoral perfusion may be related to cancer activity, as we showed.

As mentioned above, higher perfusion suggests the lower presence of stroma. Reports indicate that poor tumor perfusion is among the factors leading to PDA chemoresistance [4, 10]. As previous study using perfusion MRI reported pathologically [6], the presence of a prominent stromal matrix reduces blood vessel density in PDA tissue. A previous study [10] showed that depletion of tumor associated stromal matrix, using the inhibitor of hedgehog signaling pathway through effect on Smo, increased vasculature and concentration of drug in the tumor tissue and approved prognosis. Beatty et al. also showed that depleting the tumor stroma via activated macrophages using an agonist CD40 antibody improved prognosis in a genetically engineered mouse model of PDA [20]. However, our present study found tumor blood flow unrelated to prognosis. Our evaluation accounted for only one perfusion parameter: tumor blood flow. In fact, there are several perfusion parameters, including tissue blood flow, blood volume, and permeability [21]. Park et al. report that decreased tumor permeability measured by perfusion CT is related to chemosensitivity [22]. Thus, our study leaves open the possibility that another tumoral perfusion parameter may be related to prognosis.

Our investigation presents the following potential limitations. First, while we used the patient survival days as an index of prognosis, prognosis is not necessarily equivalent to chemosensitivity; we did not assess the relationship between perfusion in the tissue surrounding cancer and response rate to gemcitabine. Second, we defined the tissue surrounding cancer as pancreatic tissue within 10 mm of the juxtaposed proximal pancreatic parenchyma. While we assumed this tissue was composed of normal pancreatic tissue, it is certainly possible that it contained a marginal zone of cancerous tissue. Third, we used the software developed by Ziosoft, but differences of perfusion parameters between software programs or their upgrades have been reported, recently [23]. Therefore,

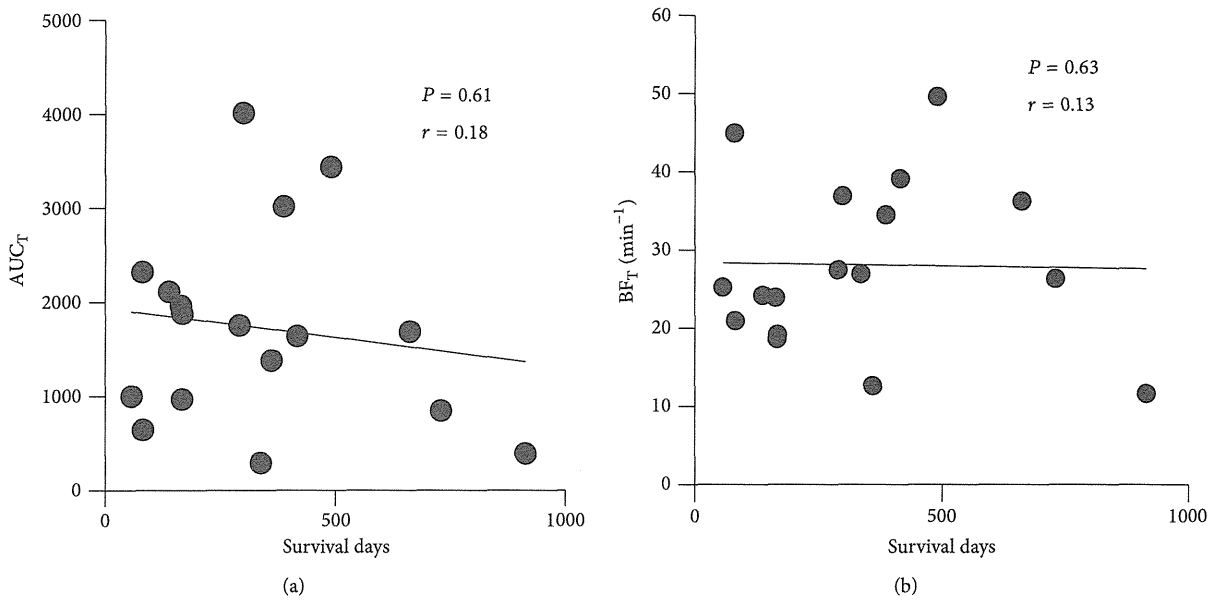

FIGURE 2: Relationship between AUC_T or BF_T and survival days. Panels (a) and (b) show the relationship between survival days and pancreatic AUC_T or BF_T, respectively.

our results could change by analyzing other software. Lastly, our study was a pilot study enrolling a limited number of patients.

5. Conclusion

Patient prognosis may be related to perfusion in tissue surrounding pancreatic cancer observed with perfusion CT.

Conflict of Interests

The authors declare that there is no conflict of interests regarding the publication of this paper.

References

[1] A. Jemal, R. Siegel, J. Xu, and E. Ward, "Cancer statistics, 2010," *CA Cancer Journal for Clinicians*, vol. 60, no. 5, pp. 277–300, 2010.

[2] N. Bardeesy and R. A. DePinho, "Pancreatic cancer biology and genetics," *Nature Reviews Cancer*, vol. 2, no. 12, pp. 897–909, 2002.

[3] M. Malvezzi, A. Arfé, P. Bertuccio, F. Levi, C. La Vecchia, and E. Negri, "European cancer mortality predictions for the year 2011," *Annals of Oncology*, vol. 22, no. 4, pp. 947–956, 2011.

[4] H. A. Burris III, M. J. Moore, J. Andersen et al., "Improvements in survival and clinical benefit with gemcitabine as first-line therapy for patients with advanced pancreas cancer: a randomized trial," *Journal of Clinical Oncology*, vol. 15, no. 6, pp. 2403–2413, 1997.

[5] M. Hidalgo, "Pancreatic cancer," *The New England Journal of Medicine*, vol. 362, pp. 1605–1617, 2010.

[6] M. A. Bali, T. Metens, V. Denolin et al., "Tumoral and non-tumoral pancreas: correlation between quantitative dynamic contrast-enhanced MR imaging and histopathologic parameters," *Radiology*, vol. 261, no. 2, pp. 456–466, 2011.

[7] M. Erkan, J. Kleeff, A. Gorbachevski et al., "Periostin creates a tumor-supportive microenvironment in the pancreas by sustaining fibrogenic stellate cell activity," *Gastroenterology*, vol. 132, no. 4, pp. 1447–1464, 2007.

[8] M. A. Jacobetz, D. S. Chan, A. Neesse et al., "Hyaluronan impairs vascular function and drug delivery in a mouse model of pancreatic cancer," *Gut*, vol. 62, no. 1, pp. 112–120, 2013.

[9] A. B. Lowenfels, P. Maisonneuvi, G. Cavallini et al., "Pancreatitis and the risk of pancreatic cancer," *New England Journal of Medicine*, vol. 328, no. 20, pp. 1433–1437, 1993.

[10] K. P. Olive, M. A. Jacobetz, C. J. Davidson et al., "Inhibition of Hedgehog signaling enhances delivery of chemotherapy in a mouse model of pancreatic cancer," *Science*, vol. 324, no. 5933, pp. 1457–1461, 2009.

[11] A. Radu, C. Pichon, P. Camparo et al., "Expression of follicle-stimulating hormone receptor in tumor blood vessels," *The New England Journal of Medicine*, vol. 363, no. 17, pp. 1621–1630, 2010.

[12] M. A. Mazzei, N. C. Squitieri, S. Guerrini et al., "Quantitative CT perfusion measurements in characterization of solitary pulmonary nodules: new insights and limitations," *Recenti Progressi in Medicina*, vol. 104, no. 7, pp. 430–437, 2013.

[13] F. T. Bosman, F. Carneiro, R. H. Hruban et al., *WHO Classification of Tumours of the Digestive System, Fourth Edition*, IARC Press, Lyon, France, 2010.

[14] The Japan Pancreas Society, *Classification of Pancreatic Carcinoma*, Kanehara, 3rd English edition, 2011.

[15] Y. Tsuji, H. Yamamoto, S. Yazumi, Y. Watanabe, K. Matsueda, and T. Chiba, "Perfusion computerized tomography can predict pancreatic necrosis in early stages of severe acute pancreatitis," *Clinical Gastroenterology and Hepatology*, vol. 5, no. 12, pp. 1484–1492, 2007.

[16] Y. Tsuji, K. Koizumi, H. Isoda et al., "The radiological exposure of pancreatic perfusion computed tomography," *Pancreas*, vol. 39, no. 4, pp. 541–543, 2010.

[17] R. G. Sheiman and A. Sitek, "Feasibility of measurement of pancreatic perfusion parameters with single-compartment kinetic model applied to dynamic contrast-enhanced CT images," *Radiology*, vol. 249, no. 3, pp. 878–882, 2008.

[18] K. A. Miles and M. R. Griffiths, "Perfusion CT: a worthwhile enhancement?" *The British Journal of Radiology*, vol. 76, no. 904, pp. 220–231, 2003.

[19] G. A. Zamboni, L. Bernardin, and R. Pozzi Mucelli, "Dynamic MDCT of the pancreas: is time-density curve morphology useful for the differential diagnosis of solid lesions? A preliminary report," *European Journal of Radiology*, vol. 81, no. 3, pp. e381–e385, 2012.

[20] G. L. Beatty, E. G. Chiorean, M. P. Fishman et al., "CD40 agonists alter tumor stroma and show efficacy against pancreatic carcinoma in mice and humans," *Science*, vol. 331, no. 6024, pp. 1612–1616, 2011.

[21] K. A. Miles, "Perfusion CT for the assessment of tumour vascularity: which protocol?" *British Journal of Radiology*, vol. 76, no. 1, pp. S36–S42, 2003.

[22] M.-S. Park, E. Klotz, M.-J. Kim et al., "Perfusion CT: Noninvasive surrogate marker for stratification of pancreatic cancer response to concurrent chemo—and radiation therapy," *Radiology*, vol. 250, no. 1, pp. 110–117, 2009.

[23] M. A. Mazzei, N. C. Squitieri, E. Sani et al., "Differences in perfusion ct parameter values with commercial software upgrades: a preliminary report about algorithm consistency and stability," *Acta Radiologica*, vol. 54, no. 7, pp. 805–811, 2013.

HEPATOLOGY
Official Journal of the American Association for the Study of Liver Diseases

Progression of Autoimmune Hepatitis is Mediated by IL-18-Producing Dendritic Cells and Hepatic CXCL9 Expression in Mice

Aki Ikeda,[1,2]* Nobuhiro Aoki,[1,2]* Masahiro Kido,[1,2]* Satoru Iwamoto,[1,2] Hisayo Nishiura,[1,2] Ryutaro Maruoka,[1,2] Tsutomu Chiba,[2] and Norihiko Watanabe[1,2]

Clinical manifestations of autoimmune hepatitis (AIH) range from mild chronic to acute, sometimes fulminant hepatitis. However, it is unknown how the progression to fatal hepatitis occurs. We developed a mouse model of fatal AIH by inducing a concurrent loss of forkhead box $P3^+$ regulatory T cells and programmed cell death-1 (PD-1)-mediated signaling. In this model, dysregulated follicular helper T cells in the spleen are responsible for the induction, and the C-C chemokine receptor 6/C-C chemokine ligand 20 axis is crucial for the migration of these T cells into the liver. Using this fatal AIH model, we aimed to clarify key molecules triggering fatal AIH progression. During progression, T-bet together with interferon (IFN)-γ and C-X-C chemokine receptor (CXCR)3 were highly expressed in the inflamed liver, suggesting helper T (Th)1-type inflammation. T cells that dominantly expanded in the spleen and the inflamed liver were CXCR3-expressing $CD8^+$ T cells; depletion of these $CD8^+$ T cells suppressed AIH progression. Expression of one CXCR3 ligand, chemokine (C-X-C motif) ligand (CXCL)9, was elevated in the liver. CXCL9-expressing macrophages/Kupffer cells were colocalized with infiltrating T cells, and *in vivo* administration of anti-CXCL9 suppressed AIH progression. In addition, serum levels of interleukin (IL)-18, but not IL-1β, were elevated during progression, and dendritic cells in the spleen and liver highly produced IL-18. *In vivo* administration of anti-IL-18R suppressed the increase of splenic $CXCR3^+$ T cells and the progression to fatal AIH. Moreover, tumor necrosis factor alpha, but not IFN-γ, was involved in up-regulating CXCL9 in the liver and for increased serum levels of IL-18. *Conclusion:* These data suggest that, in our mouse model, fatal progression of AIH is mediated by IL-18-dependent differentiation of T cells into Th1 cells and effector T cells, respectively, and that CXCR3-CXCL9 axis-dependent migration of those T cells is crucial for fatal progression. (HEPATOLOGY 2014;60:224-236)

Human autoimmune hepatitis (AIH) typically presents as asymptomatic or mild chronic hepatitis. However, presentation as acute severe hepatitis also occurs, and some of these AIH patients manifest liver failure at initial presentation.[1,2] Untreated patients with severe AIH rapidly decline, with a mortality rate of up to 50% from 3 to 5 years after diagnosis.[3] Patients progressing to acute liver failure respond poorly to corticosteroid treatment, some of them needing liver transplantation (LT).[4,5] In addition, approximately 20%-30% of patients undergoing LT for AIH develop features of recurrent disease; in

Abbreviations: Ab, antibody; AIH, autoimmune hepatitis; ANA, antinuclear antibody; ALT, alanine aminotransferase; AST, aspartate aminotransferase CCL, C-C chemokine ligand; CCR, C-C chemokine receptor; CNS, central nervous system; CXCL, chemokine (C-X-C motif) ligand; CXCR, C-X-C chemokine receptor; DCs, dendritic cells; EAE, experimental autoimmune encephalomyelitis; ELISA, enzyme-linked immunosorbent assay; FCM, flow cytometry; GC, germinal center; ICOS, inducible costimulator; IFN-γ, interferon-gamma; Ig, immunoglobulin; IHC, immunohistochemistry; IL, interleukin; IL-21R, IL-21 receptor; IP, intraperitoneally; KCs, Kupffer cells; LT, liver transplantation; mAb, monoclonal Ab; MC, mononuclear cell; MLNs, mesenteric lymph nodes; mRNA, messenger RNA; NALP3, NACHT, LRR, and pyrin domain-containing protein 3; NK, natural killer; NTx, neonatal thymectomy; NTx–$PD1^{-/-}$ mice, PD-1-deficient BALB/c mice thymectomized 3 days after birth; PD-1, programmed cell death 1; qRT-PCR, quantitative reverse-transcriptase polymerase chain reaction; r, recombinant; T_{FH}, follicular helper T; Th, helper T; TNF-α, tumor necrosis factor alpha; Tregs, regulatory T cells.

From the [1]Center for Innovation in Immunoregulative Technology and Therapeutics and [2]Department of Gastroenterology and Hepatology, Graduate School of Medicine, Kyoto University, Kyoto, Japan.

Received August 2, 2013; accepted February 19, 2014.

some, recurrent AIH behaves more aggressively, with progression to cirrhosis and graft failure.[6] However, it is unknown how this progression to fatal hepatic damages occurs.

Recently, we developed a mouse model of spontaneous fatal AIH.[7-11] Neither *programmed cell death-1* (*PD-1*)-deficient mice (*PD-1*$^{-/-}$ mice) nor BALB/c mice thymectomized 3 days after birth (NTx mice) developed any inflammation of the liver. However, in *PD-1*$^{-/-}$ BALB/c mice with neonatal thymectomy (NTx–*PD-1*$^{-/-}$ mice), immune dysregulation by a concurrent loss of naturally arising forkhead box P3^{+} regulatory T cells (Tregs) and PD-1-mediated signaling induced fatal AIH. Massive destruction of the parenchyma of the liver resulted in most mice dying by 4 weeks. Fatal AIH in NTx–*PD-1*$^{-/-}$ mice was characterized by CD4^{+} and CD8^{+} T-cell infiltration with massive lobular necrosis in the liver and by hypergammaglobulinemia and production of antinuclear antibodies (ANAs).[7,8]

In our mouse model of fatal AIH, we identified induction sites, responsible T-cell subsets, and key molecules for induction of AIH.[8] The spleen is an induction site for fatal AIH, and splenic CD4^{+} T cells were autonomously differentiated into follicular helper T (T_{FH}) cells in 2-week-old NTx–*PD-1*$^{-/-}$ mice. T_{FH} cells expressing Bcl6, interleukin (IL)−21, IL-21 receptor, inducible costimulator (ICOS), and C-X-C chemokine receptor (CXCR)5 comprise a newly defined effector T-cell subset that powerfully assists B cells in forming germinal centers (GCs).[12] Indeed, in NTx–*PD-1*$^{-/-}$ mice, the dysregulated T_{FH} cells promoted hypergammaglobulinemia and ANA production. In addition, these T_{FH} cells in the spleen directly migrated into the liver through the C-C chemokine receptor 6/C-C chemokine ligand 20 (CCR6-CCL20) axis, triggering induction of fatal AIH.[8]

On the other hand, in the progression phase of AIH in 3-week-old NTx–*PD-1*$^{-/-}$ mice, infiltrated CD4+ and CD8+ T cells in the liver produced large amounts of inflammatory cytokines, such as interferon-gamma (IFN-γ) and tumor necrosis factor alpha (TNF-α).[7,8] Therefore, dysregulated T_{FH} cells in the induction and helper T (Th)1 cells with effector CD8^{+} T cells in the progression may play their roles at different time points in development of fatal AIH. In this study, using our mouse model, we examined mechanisms in the progression process to identify key molecules triggering fatal AIH progression. We found that in the progression, CXCR3-expressing Th1 cells and CD8^{+} effector T cells infiltrated in the liver, with CD8^{+} effector T cells triggering the fatal destruction of the liver, that hepatic macrophages/Kupffer cells (KCs) producing chemokine (C-X-C motif) ligand (CXCL)9 is critical for migration of these T cells, and that dendritic cell (DC)-derived IL-18 is critical for differentiation of Th1 cells and CD8^{+} effector T cells. These data suggest that in this mouse model of AIH, IL-18 and the CXCR3/CXCL9 axis are critical for T-cell differentiation and migration in fatal progression of AIH.

Materials and Methods

BALB/c mice were purchased from Japan SLC (Shizuoka, Japan), and *PD-1*$^{-/-}$ on a BALB/c background were generated as described previously.[13] These mice were bred and housed under specific pathogen-free conditions. Thymectomies were performed as described.[7-11] All mouse protocols were approved by the Institute of Laboratory Animals, Graduate School of Medicine, Kyoto University (Kyoto, Japan).

All other protocols for histological and immunohistological (IHC) analysis, real-time quantitative reverse-transcription polymerase chain reactions (qRT-PCR), flow cytometry (FCM) analysis and isolation of single cells, administration of antibodies (Abs) *in vivo*, enzyme-linked immunosorbent assay (ELISA), *in vivo* injection of cytokines, DC coculture, and statistical analysis are detailed in the Supporting Materials and Methods.

The Center for Innovation in Immunoregulative Technology and Therapeutics is supported, in part, by the Special Coordination Funds for Promoting Science and Technology of the Japanese Government and, in part, by Astellas Pharma Inc. in the Formation of the Innovation Center for Fusion of Advanced Technologies Program. This work is partially supported by Grants-in-Aid for Scientific Research (20390207, 21229009, and 23590973) from the Japan Society for the Promotion of Science, a Health and Labor Sciences Research Grant for Research on Intractable Diseases, and Research on Hepatitis from the Ministry of Health, Labor and Welfare, Japan, Grants-in-Aid for Research by The Kato Memorial Trust for Nambyo Research, and The Waksman Foundation of Japan.

**These authors contributed equally to this work.*

Address reprint requests to: Norihiko Watanabe, M.D., Ph.D., Kyoto University, Yoshida-Konoe-Cho, Sakyo-Ku, Kyoto City, Kyoto 606-8501, Japan. E-mail: norihiko@kuhp.kyoto-u.ac.jp; fax: +81-75-751-4303.

View this article online at wileyonlinelibrary.com.

DOI 10.1002/hep.27087

Potential conflict of interest: Nothing to report.

Results

T-bet, IFN-γ, and CXCR3 Are Highly Up-Regulated in Inflamed Livers of 3-Week-Old NTx-PD-1$^{-/-}$ Mice. In our mouse model, AIH induction was started as early as 2 weeks of age by dysregulated T_{FH} cells in the spleen.[7,8] Livers in 2-week-old NTx–*PD-1*$^{-/-}$ mice showed mononuclear cell (MC) infiltrations, predominantly in the portal area, as previously described (Fig. 1A).[7] Within 7 days of induction, these MC infiltrations rapidly progressed and were followed by massive destruction of the parenchyma of the liver (Fig. 1A). To investigate whether cytokines contributed to the severely inflamed livers of these 3-week-old NTx–*PD-1*$^{-/-}$ mice, we performed real-time qRT-PCR analysis to measure the expression levels of messenger RNA (mRNA) encoding T-cell lineage-specific transcription factors and various related cytokines. In contrast to expression of Th2 or Th17-related molecules, expression of Th1 lineage-specific transcription factor T-bet, together with IFN-γ and TNF-α, were up-regulated in inflamed liver tissues of these mice (Fig. 1B). These data suggest that inflammatory cytokines related to Th1-type inflammation may be involved in fatal progression of AIH. Notably, we found that in the inflamed livers of these mice, mRNA expressions of CXCR3 were highly up-regulated along with Th1-related molecules (Fig. 1C). Although AIH induction was mediated by dysregulated T_{FH} cells in the spleen, in the progression phase of AIH, Th1-type responses were predominant.

T Cells Dominantly Expanded in the Inflamed Liver Were CXCR3-Expressing CD8$^+$ T Cells. Next, we monitored T-cell numbers of the liver, spleen, and mesenteric lymph nodes (MLNs) in NTx–*PD-1*$^{-/-}$ mice from 1 to 3 weeks of age (Fig. 1D). In the AIH progression phase in 3-week-old mice, we found that CD8$^+$ T cells, and, to a lesser extent, CD4$^+$ T cells, extensively increased in the liver, as described previously.[7] Notably, the predominant increase of CD8$^+$ T cells at 3 weeks was observed only in the liver, but not in the spleen or MLNs (Fig. 1D), implying that CD8$^+$ T cells had accumulated in the severely inflamed liver. In addition, we analyzed splenic and hepatic CD8$^+$ T-cell expression of the chemokine receptors, CCR6, CCR9, and CXCR3, by FCM. As with CD4$^+$ T cells in the spleen and liver,[8] splenic and hepatic CD8$^+$ T cells mainly expressed CXCR3 in 3-week-old NTx–*PD-1*$^{-/-}$ mice (Fig. 1E).

CD8$^+$ T Cells During Progression of AIH Were Indispensable for Fatal Destruction of the Liver. In a previous study, we showed that in the induction of fatal AIH, CD4$^+$ T cells are indispensable for recruiting CD8$^+$ T cells in the liver and that CD8$^+$ T cells may be major effector T cells, fatally destroying the liver in AIH progression.[8] To examine whether depletion of CD8$^+$ T cells in the progression is sufficient to suppress fatal liver destruction, AIH-developed NTx–*PD-1*$^{-/-}$ mice were injected intraperitoneally (IP) at 14 days after NTx and then once a week with anti-CD8 monoclonal Abs (mAbs) *in vivo* (Fig. 2A). After two injections of anti-CD8, the number of CD8$^+$ T cells in the spleen was greatly reduced (Fig. 2B). Although depleting CD8$^+$ T cells did not completely suppress hepatic infiltrations of MCs, infiltration of CD4$^+$ and CD8$^+$ T cells was diminished, and fatal progression of AIH was suppressed by the treatment (Fig. 2C-E). These data suggest that CXCR3-expressing CD8$^+$ T cells extensively infiltrating the liver are indispensable for fatal progression.

Production of a CXCR3 Ligand, CXCL9, Was Elevated in Fatal Progression of AIH. CXCR3-expressing T cells can be guided by three ligands—CXCL9/monokine induced by IFN-γ (MIG), CXCL10/IFN-inducible protein 10 (IP10), and CXCL11/IFN-inducible T cell alpha chemoattractant (I-TAC)—and expression of these CXCR3 ligands in the inflamed tissues determines inflamed-tissue–specific infiltration of CXCR3-expressing T cells in various immunoinflammatory settings, including autoimmune diseases.[14-17] We performed real-time qRT-PCR analysis to measure expression levels of mRNA encoding these three CXCR3 ligands. In contrast to noninflamed livers in control mice, severely inflamed livers of 3-week-old NTx–*PD-1*$^{-/-}$ mice showed markedly elevated gene expression of CXCL9, but not of CXCL10 and CXCL11 (Fig. 3A). In contrast to inflamed livers, no organs, except those with inflamed gastric tissues, showed a significantly increased level of mRNA expression of CXCL9 (Fig. 3B).

In addition, we confirmed elevated protein expression of CXCL9 only in the inflamed liver, but not the stomach, by IHC (Fig. 3C and Supporting Fig. 1). Furthermore, when we looked at serum concentrations of CXCL9 and CXCL10 at 1-4 weeks of age, serum level of CXCL9, but not CXCL10, at 3-4 weeks of age, was significantly higher than controls (Fig. 3D). These data suggest that CXCL9 plays a key role in progression of AIH.

In Fatal Progression of AIH, the CXCR3-CXCL9 Axis Was Crucial for T-Cell Migration Into the Liver. To determine whether the axis formed by CXCR3 and its ligands contributes to T-cell migration leading to fatal progression of AIH, NTx–*PD-1*$^{-/-}$ mice were injected IP at 1 day after NTx and then